Journal of Statistical Physics, Vol. 95, Nos. 5/6, 1999

Wetting of Alkanes on Water from a Cahn-Type Theory: Effects of Long-Range Forces

Joseph O. Indekeu,[1] Karine Ragil,[2] Daniel Bonn,[3] Daniel Broseta,[2] and Jacques Meunier[3]

Received February 25, 1998; final June 15, 1998

We apply the phenomenological wetting theory of Cahn to fluids with van der Waals forces, and in particular to the wetting of pentane on water. Taking into account explicitly the long-range substrate–adsorbate interaction allows us to reproduce the experimentally observed critical wetting transition, which arises from the vanishing of the Hamaker constant at $T \approx 53°C$. This transition is preceded by a first-order transition between a thin and a thick film at a (much) lower temperature. If long-range forces are neglected, this thin–thick transition is the only wetting transition and critical wetting is missed. Our study focuses on the development of useful theoretical tools, such as phase portraits and interface potentials adapted to systems with van der Waals forces.

KEY WORDS: Wetting phase transitions; alkanes; long-range forces.

1. INTRODUCTION

In this paper we apply the phenomenological wetting theory of Cahn[(1)] to systems in which the long-range (i.e., decaying as an inverse power of distance) interactions between molecules are important for the wetting properties. In most of the systems studied so far, the wetting behavior displays a first-order (discontinuous) transition between a thin and a thick adsorbed film when varying the temperature T, for instance. This transition is usually treated within the frame-work of the standard Cahn theory, which only takes into account short-range substrate-adsorbate forces. The

[1] Laboratorium voor Vaste-Stoffysica en Magnetisme, Katholieke Universiteit Leuven, B-3001 Leuven, Belgium.
[2] Institut Français du Pétrole, F-92500 Rueil-Malmaison, France.
[3] Laboratoire de Physique Statistique, Ecole Normale Supérieure, 24, F-75231 Paris Cedex 05, France.

0022-4715/99/0600-1009$16.00/0

wetting behavior of light alkanes (e.g., pentane, hexane,...) on water is, however, more complex. These systems display a critical (continuous) wetting transition between a thin and a thick film, upon increasing T. This transition, first observed for pentane on water, is due to the vanishing of the Hamaker constant,[2] and cannot be understood on the basis of the standard theory.

At some lower temperature another first-order transition takes place between the above thin film, which turns out to be of mesoscopic thickness, and a microscopically thin film, upon lowering T. This first-order transition, first observed for hexane on brine,[3] is reminiscent in temperature location and in discontinuous character of the first-order wetting transition found in the standard Cahn theory. However, the system remains in a partial wetting state on both sides of the transition.

This unusual wetting behavior has been attributed to the competition between short-and long-range forces which, in the interval between the two transitions, inhibits the growth of a macroscopic wetting layer required for complete wetting. The Hamaker constant, which is proportional to the net van der Waals force between the interfaces bounding the wetting film, varies continuously and vanishes at a somewhat larger temperature, thus allowing the mesoscopic film to grow continuously to a macroscopic wetting layer.[2, 3]

Our purpose in this work is to account for the wetting behavior of alkanes on water by incorporating van der Waals forces into Cahn's mean-field (or Landau) theory of wetting. It is worth emphasizing that understanding and predicting the wetting properties of alkanes and, more generally, oils on water is very important from the standpoint of the oil industry, as these properties govern the fluid repartition and flow within the reservoir porous space.[4]

The approach we take is a natural extension of a previous study in which the theory (without long-range forces) was applied to alkanes on water.[5] Furthermore, in our computations the so-called dynamical analogy and the method of "phase portraits" play a central role. The use of phase portraits is non-trivial and has seldom been pursued in the presence of long-range forces, because in the dynamical analogy energy is not conserved, so that the computations are more difficult. Nevertheless, it provides a powerful means of locating wetting phase transitions, since the usual technique of inspection of the portrait geometry with the help of equal-areas rules remains an exact and systematic method even in the presence of long-range forces. Our analysis is similar to previous reasoning in the context of wetting on curved substrates[6] and wetting in type-I superconductors,[7] where the standard phase portraits are replaced by "initial-condition" portraits.

Wetting theory with long-range forces has been developed to a considerable extent, following the observation that the description of interfacial phenomena in fluids is qualitatively incorrect, if the "van der Waals tails" are neglected.[8] Furthermore, for long-range forces that favor wetting (agonistic forces) the wetting transition is of *first order*, while for long-range forces that oppose wetting (antagonistic forces) the transition is suppressed.[9] Thus, *critical wetting* was believed to be highly unlikely or even absent altogether in the presence of long-range forces. This expectation was confirmed[10] for simple "interface potentials" of the type

$$V(l) = Al^{-\sigma} \tag{1.1}$$

This potential represents the reduced free energy per unit area of a wetting layer of predetermined thickness l, so that the equilibrium thickness is found by minimizing this potential. All quantities in (1.1) are assumed to be reduced or "scaled" with appropriate constants so that they are dimensionless. The exponent σ (>0) comes from the power-law decay of the intermolecular potentials, which are integrated over $d+1$ dimensions, so that for van der Waals forces in spatial dimension $d=3$ the result is $\sigma=2$. When the amplitude A, proportional to the Hamaker constant of the system, is assumed constant, any wetting transition is of first order for $A>0$, while for $A<0$ the interface remains at finite l. This conclusion is not altered by the effect of the increasing entropy of interface fluctuations for large l, because this effect leads to modifications of $V(l)$ in the form of exponentially decaying terms only.[8]

The absence of critical wetting in systems with long-range forces was thus established, but under the assumption that the leading amplitude A is (nearly) constant. It was soon realized[11] that for simple Lennard–Jones systems, interaction potential calculations give an amplitude A that depends on *bulk polarizability densities* in a subtle way. Consequently, A cannot be assumed constant but depends on the temperature T. A more realistic interface potential therefore is

$$V(l) = A(T)\, l^{-\sigma} + B(T)\, l^{-(\sigma+1)} + \cdots \tag{1.2}$$

with $B(T)$ depending only weakly on T compared with $A(T)$. Now critical wetting is possible for $A \to -0$, in which case the wetting layer thickness diverges as $l \propto |T_w - T|^{-1}$, assuming $A \propto T - T_w$, with T_w the wetting temperature, at which the effective Hamaker constant vanishes.

At around the same time a Cahn–Landau theory for wetting with long-range forces was employed in ref. 11 (second paper), and ref. 12. This type of theory is what we work with here, but instead of adopting previously used approximations to facilitate the calculations, we deal with the

full theory numerically, employing the phase portrait method. In ref. 12 the leading amplitude of the long-range forces was assumed constant, and the aforementioned conclusions concerning the absence of critical wetting were confirmed.

At the next and more quantitative level of development of the theory a microscopic lattice-gas mean-field theory was used in which *all* interactions are long-ranged (substrate-adsorbate as well as adsorbate-adsorbate).[13] Based on this theory, an interface potential was derived and explicit forms were obtained for the leading amplitudes $A(T)$ and $B(T)$. The occurrence of a critical wetting transition was demonstrated in a model computation. Also, a first-order transition from a thin to a thick film, preceding a critical wetting transition, has been observed in this model (see Fig. 1 in the first paper of ref. 13). The conditions on the long-range forces for the critical wetting phenomenon to occur were formulated. In principle these conditions can be checked provided one can calculate all the long-range forces in detail.

In subsequent work[14] the emphasis was somewhat shifted back to a phenomenological analysis of the interface potential $V(l)$, which, although derivable explicitly from a microscopic lattice mean-field theory, can be viewed as a phenomenological expansion in the order parameter $1/l$, with temperature-dependent coefficients A, B,... in terms of which global phase diagrams can be mapped out. The goal of this analysis is to locate first-order, critical, and multicritical wetting transitions, discuss scaling relations and universal quantities such as critical exponents. Following a thorough discussion of Cahn's scaling argument for critical-point wetting in systems with long-range forces,[15] an exploration was made[16] of how long-range forces can be incorporated within the Cahn–Landau theory in order to allow a systematic calculation of global phase diagrams as was done previously for short-range forces.[17]

The work of Ebner and Saam[14] differs from the earlier analytic approach of Privman[12] in that the long-range forces are now incorporated in an effective short-range field $h_{1,\,\mathrm{eff}}$, and an effective surface enhancement g_{eff}. An important conclusion of this work is that the long-range forces can affect the phase diagrams significantly, in line with qualitative arguments put forward in previous work.[9, 15] Another crucial observation, which we also adhere to, is that it is useful and physically reasonable to work with an *effective* long-range field between substrate and adsorbate, while adsorbate-adsorbate long-range interactions are not explicitly taken into account. The theory can then be simplified to a short-range Cahn–Landau free-energy functional supplemented with an integral over the density times a long-range field $h(z)$. The reasoning behind this simplification is that taking *all* long-range forces into account leads to a net substrate-adsorbate

potential in which the coefficients of inverse powers of distance are linear combinations of the adhesive and cohesive contributions.

Our approach is close in spirit to that of Ebner and Saam. However, instead of mapping the whole problem onto a calculation with only short-range potentials, we carry out an exact analysis keeping the long-range substrate-adsorbate field as it is. This is possible by extending the phase portrait method, as we shall show in the following Section.

The remainder of this paper is organized as follows. Sections 2 to 4 are devoted to the extension of the phase portrait technique and the interface potential derivation for systems with long-range forces. Section 5, on the other hand, deals with the specific adaptation of the general methods to the concrete experimentally relevant case of, e.g., pentane on water.

2. PHASE PORTRAITS FOR LONG-RANGE FORCES

In this Section we outline some general properties of the Cahn–Landau theory including long-range forces, and employ the symmetric Ising-model representation for simplicity. Thus, the density is simply represented by an equivalent variable m, which is the order parameter (magnetization) in the model. For the reduced mean-field free-energy functional $\bar{\gamma}[m]$, with $m(z)$ the density profile, we assume

$$\bar{\gamma}[m] = \int_1^\infty dz \left\{ \frac{1}{2}\left(\frac{dm}{dz}\right)^2 + f(m) - h(z)\, m \right\} + \varphi_s(m_1) \tag{2.1}$$

The adsorbate is located in the half-space $z > 1$. The dimensionless distance z is measured in units of a microscopic length. We will henceforth assume that this length is of the order of 1 Å. The substrate or "wall" is located at $z = 1$, and may consist of a surface or interface that is sufficiently sharp on a molecular scale. The Landau bulk free energy density is modeled by $f(m)$. A convenient form is the standard quartic polynomial

$$f(m) = (m^2 - m_0^2)^2 - h_b m + c \tag{2.2}$$

where $\pm m_0$ are the equilibrium values for m at bulk two-phase coexistence, i.e., for zero bulk field, $h_b = 0$. The field h_b measures the distance from two-phase coexistence, and for a fluid corresponds to a chemical potential difference. The parameter c is adjusted so that $f = 0$ in its minimum, i.e., for $m = m_b$, the bulk equilibrium value.

The long-range substrate–adsorbate field $h(z)$ takes into account, in a first *approximation*, the net effect of the long-range interactions between substrate and adsorbate molecules.

Note that the ansatz of including a term $h(z)\,m(z)$ cannot be exact. Indeed, in this way the adsorbate–adsorbate long-range forces cannot be fully incorporated and a fluid–fluid interface far from the substrate will display exponential tails rather than realistic van der Waals tails.

For a meaningful description of the effect of long-range forces on wetting the field $h(z)$ must at least contain the leading and next-to-leading terms in the large-z expansion of the effective van der Waals interaction between an adsorbate molecule and the substrate half-space,

$$h(z) = a_3 z^{-3} + a_4 z^{-4} \tag{2.3}$$

where a_3 and a_4 are, in general, temperature-dependent.

If one considers a wetting layer of thickness l and calculates the interface potential $V(l)$ on the basis of the ansatz (2.1), one finds that the expansion of $h(z)$ for large z is simply related to the asymptotic part, for large l, of the function $\Pi(l) \equiv -dV(l)/dl$. Consequently, the coefficient a_3 is proportional to the amplitude A in (1.2) and therefore to the Hamaker constant (see Section 3 for explicit expressions).

The function $\Pi(l)$ is the disjoining pressure and is measurable experimentally for fluid interfaces. Therefore, there are two conceivable paths for estimating the leading coefficients of $h(z)$ quantitatively. One path is to rely on precise measurements of $V(l)$ for large l, if available. The other is to start from a fully microscopic theory and calculate the leading terms of $V(l)$ for a specific molecular system. A derivation of this kind, based on density functional theory for particles interacting through spherically symmetric potentials, has been given by Dietrich and Napiorkowski.[18] They provided the leading three coefficients of $V(l)$.

Even if we were able to generalize this microscopic approach to our fairly complex system of *non-spherical* molecules, precise knowledge of $V(l)$ for small l would still be lacking. The square-gradient theory assumed in (2.1) provides additional information about the behavior of $V(l)$ at small l, and in this sense it can be regarded as complementary to the approach of ref. 18. However, the best we can hope for, using (2.1), is to obtain qualitative insight in $V(l)$ for small l, since practically all microscopic details of the system influence the short-range behavior of $V(l)$ and thus affect the precise location of first-order adsorption transitions in general.

Finally, the short-range substrate–adsorbate interaction is incorporated in the surface contact potential $\varphi_s(m_1)$ with $m_1 \equiv m(z=1)$. Usually, $\varphi_s(m_1)$ is taken to be a (second-order) polynomial $-h_1 m_1 - g m_1^2/2$, but for our purposes φ_s can be a more general function, which we do not need to specify at present. Unless stated otherwise, we shall henceforth assume that the system is at bulk coexistence, i.e., $h_b = 0$, and $m_b = \pm m_0$. For concrete-

ness, we will associate $m_b = -m_0$ with the bulk gas phase (G) and $m_b = m_0$ with the bulk liquid phase (L).

The density profile $m(z)$ which extremizes the functional obeys the Euler–Lagrange "equation of motion,"

$$\ddot{m} = \frac{df}{dm} - h(z) \tag{2.4}$$

where the dot stands for d/dz. In the dynamical analogy[19] z is the time and m the position of a particle that moves in the potential $U = -f(m)$, which has the shape of a double hill. The particle is furthermore acted upon by a time-dependent force proportional to $h(z)$. The particle moves over the double hill and is required to come to a stop on one of the hilltops, according to the bulk condition or "final" condition

$$m(z) \to m_b, \qquad \text{for} \quad z \to \infty \tag{2.5}$$

Furthermore, extremalization of the functional with respect to the wall value m_1 leads to the wall boundary condition or "initial" condition

$$\dot{m}(1) \equiv \dot{m}|_{z=1} = \frac{d\varphi_s}{dm_1} \tag{2.6}$$

The "trajectory" of the particle, $m(z)$, is determined by the initial conditions $m(1)$ and $\dot{m}(1)$. Depending on these the particle typically ends up in one of the three following states: (1) escape to $m = -\infty$, (2) escape to $m = \infty$, or (3) permanent oscillation between the two hilltops. As already mentioned we need those trajectories that end up precisely on a hilltop, which for $z \to \infty$ is a fixed point of the motion. The equation of motion (2.4) is nontrivial and cannot be integrated (to obtain the "constant of the motion") because h depends on z. This signifies that the particle energy is not conserved. Depending on the sign of h the particle experiences a forwards or backwards force, which helps or hinders it in reaching the hilltop. The strength of this extra force diminishes as "time" progresses, and eventually vanishes. It is this complication which necessitates the study of the "initial-condition" phase portrait instead of the usual one derived on the basis of the constant of the motion.

The initial conditions $(m_1, \dot{m}(1))$ of trajectories $m(z)$ that eventually come to a stop on one of the hilltops, say $m = -m_0$ or "G," lie on a smooth curve in the $(m, \dot{m})$-plane. We denote this curve by $Y_s^{(G)}$. Likewise, there exists $Y_s^{(L)}$. These curves are in general single- or double-valued, when considered as a function of m. Note that the trajectories considered

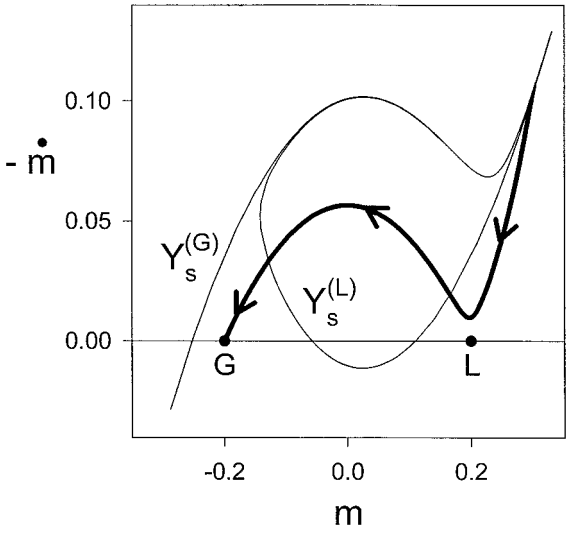

Fig. 1. Computed phase portrait in the variables m and $-\dot{m}$, for long-range field amplitudes $a_3 = -0.1$ and $a_4 = 0$, corresponding to a long-range force which prevents complete wetting. The liquid (L) and gas (G) fixed points are at $\dot{m} = 0$ and, respectively, $m = \pm m_0$. The initial conditions, at "time" $z = 1$, of trajectories that end in G lie on the curve $Y_s^{(G)}$. Likewise, trajectories that end in L start on $Y_s^{(L)}$. The latter curve makes a loop and bends back on itself (see Fig. 2 for the topology). Note that, for $m > 0$, $Y_s^{(G)}$ and the upper branch of $Y_s^{(L)}$ are nearly degenerate. The thick line (with arrows) shows an actual trajectory, which departs from a point on $Y_s^{(G)}$, and thus stops in G.

here are *not* required to satisfy the wall boundary condition (2.6) This condition will be imposed at a later stage.

The initial-condition curves $Y_s^{(G)}$ and $Y_s^{(L)}$ contain essential information on the possible phase transitions of the system, as we shall show. Besides these curves, it is also useful to visualize an actual trajectory in the phase portrait. Figure 1 shows a computed phase portrait, featuring $Y_s^{(G)}$, $Y_s^{(L)}$ (thin lines) and a typical trajectory (thick line with arrows) for a particular choice of system parameters. Note that the ordinate is chosen to be $-\dot{m}$ in place of $\dot{m}$, so that the trajectories in the upper half plane run from the right to the left.

In view of the near-degeneracy of $Y_s^{(G)}$ and $Y_s^{(L)}$, Fig. 1 cannot give a clear picture of the phase-portrait topology. In order to do justice to this aspect, we move the curves farther apart artificially and sketch, in Fig. 2, how the phase plane is divided into different regions according to the asymptotic particle motion for large times, and how $Y_s^{(L)}$ bends back on itself in the shape of a golf club.

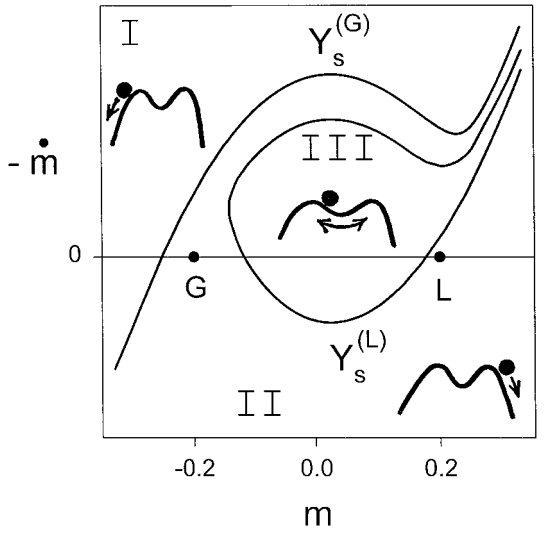

Fig. 2. Sketch of the "golf club" topology of the phase portrait of Fig. 1. The initial-condition curves are artificially moved apart in order to resolve the near-degeneracy in the upper right corner. This distorted representation allows one to distinguish the three separate regions, associated with different *asymptotic* behavior for "time" $z \to \infty$, of the trajectories that *start* in these regions. Trajectories originating in region I eventually escape to $m \to -\infty$, while those that depart from region II escape to $m \to \infty$. Region III produces trapped trajectories that oscillate indefinitely. This behavior is illustrated through the dynamical analogy of a particle moving in a double-hill potential, and eventually falling off to the left or the right, or being trapped in perpetual periodic motion (see insets). Note that the initial condition curves Y_s play the role of separatrices at $z = 1$, but for "later times" $z > 1$ trajectories may cross these curves. See ref. 30 for a good textbook on the qualitative study of nonlinear differential equations using the phase-plane or phase-portrait technique.

Now we turn to the free energy and the phase transitions. To keep the arguments simple, we will consider a single-valued initial-condition curve Y_s, such as, e.g., $Y_s^{(G)}$ in Fig. 1. (Generalization to the double-valued case is straightforward by repeating the argument for each single-valued branch and summing up the contributions of the branches). So, we consider the *function* $Y_s(m)$, which by definition associates the derivative $\dot{m}(1) \equiv -Y_s(m_1)$ to the initial value m_1. The trajectories under consideration all satisfy the equation of motion and lead to the same bulk value at "time" infinity. Therefore, the surface free energy associated with Y_s can be written as a *function* $\gamma(m_1)$, defined as the value of the functional $\bar{\gamma}[m]$ for the trajectory $m(z)$ that starts from m_1. In view of (2.1) we have

$$\gamma(m_1) = \mathscr{D}(m_1) + \varphi_s(m_1) \tag{2.7}$$

where $\mathscr{D}$ represents the integral in (2.1), evaluated for the trajectory under consideration.

At this point we recall the wall boundary condition. This condition expresses that the free energy is extremal with respect to variations of m_1, and therefore (2.6) coincides with the requirement

$$\frac{d\gamma(m_1)}{dm_1} = 0 \tag{2.8}$$

or, using (2.7),

$$-\frac{d\mathscr{D}(m_1)}{dm_1} = \frac{d\varphi_s(m_1)}{dm_1} \tag{2.9}$$

This relation is necessarily equivalent to the previously obtained expression (2.6). As a consequence, since the equivalence holds for any arbitrary choice of the function φ_s, the functions on the left hand side of (2.6) and (2.9) must be identical functions of m_1. We conclude

$$\frac{d\mathscr{D}(m_1)}{dm_1} = Y_s(m_1) \tag{2.10}$$

The importance of this identity will become clear in the context of determining possible phase transitions, an issue to which we now turn.

Determining the location of phase transitions involves calculating differences in free energy of extremal density profiles. Consider trajectories that satisfy all extremality conditions, the equation of motion (2.4), the bulk condition (2.5), as well as the wall boundary condition (2.6). Suppose that $m_1 < M_1$ are the initial values of two distinct extremal trajectories. We then have, using (2.7),

$$\begin{aligned}\gamma(M_1) - \gamma(m_1) &= \int_{m_1}^{M_1} \frac{d\mathscr{D}(m)}{dm}\, dm + \int_{m_1}^{M_1} \frac{d\varphi_s(m)}{dm}\, dm \\ &= \int_{m_1}^{M_1} Y_s(m)\, dm + \int_{m_1}^{M_1} \frac{d\varphi_s(m)}{dm}\, dm \end{aligned} \tag{2.11}$$

Clearly, this expression gives the *area* in the phase plane, enclosed between the curves Y_s and $-\varphi_s' \equiv -d\varphi_s/dm$. If the two curves cross in the interval under consideration, the enclosed area consists of two contributions of opposite sign. If, by tuning the system parameters, these contributions can be made to cancel, the free energies of the two distinct profiles are equal.

This is the mechanism for a *first-order* phase transition between surface states.

The equal-areas rule we have derived remains valid when Y_s is multi-valued, and also when $Y_s^{(G)}$ and $Y_s^{(L)}$ are combined in the sense that m_1 pertains to a point on the former and M_1 to a point on the latter. In that case the area enclosed between $Y_s^{(G)}$ and $Y_s^{(L)}$ comes into play, and contains a very narrow tongue or filament (of almost zero area) in the region where the curves are almost degenerate. We will see an example of this when we illustrate a first-order wetting transition.

The location of *critical* wetting transitions is more subtle and involves inspection of the phase portrait evolution, as a function of one of the system parameters such as the temperature, or a long-range field amplitude, such as a_3 in (2.3). The mechanism responsible for the continuous transition is the incipient degeneracy of $Y_s^{(G)}$ and $Y_s^{(L)}$. This is very different from the case of short-range forces, where critical wetting arises in connection with a point where $Y_s^{(G)}$ and $Y_s^{(L)}$ coincide.[20, 21] We will come back to critical wetting in more detail in the next Section.

3. FIRST-ORDER WETTING AND CRITICAL WETTING

As reviewed in the introduction, previous work has demonstrated that (weak) long-range forces that oppose wetting for large z (the "antagonist case"[9]) inhibit the formation of a macroscopically thick wetting layer. Thus, first-order wetting transitions are turned into first-order transitions reminiscent of prewetting, in which the thick film is of mesoscopic thickness. In contrast, long-range forces that favour wetting for large z ("agonist" case) reinforce a first-order wetting transition. In both cases critical wetting is absent, *unless* the asymptotic behavior of $h(z)$ can be tuned, in a continuous way, from antagonist to agonist. That corresponds to changing the sign of the leading amplitude a_3, which is proportional to the Hamaker constant of the system.[2]

In the following we illustrate the phase portrait analysis for the three main phenomena: a thin–thick transition, a critical wetting transition, and a first-order wetting transition. Figure 3 shows the phase portrait for $a_3 = -0.05$ and $a_4 = 0.15$. The surface contact potential is for simplicity chosen to be a second-order polynomial, and furthermore such that its derivative $-\varphi_s' = -d\varphi_s/dm$ intersects the initial condition curve $Y_s^{(G)}$ in three points. The outermost two of these intersections correspond to (local) minima of the surface free energy, associated with the thin and the thick film. The trajectories are also shown (thick lines with arrows). Note that the thick-film trajectory passes close to, but does not quite reach, the liquid fixed point L, signifying the presence of a wetting film of finite thickness. The

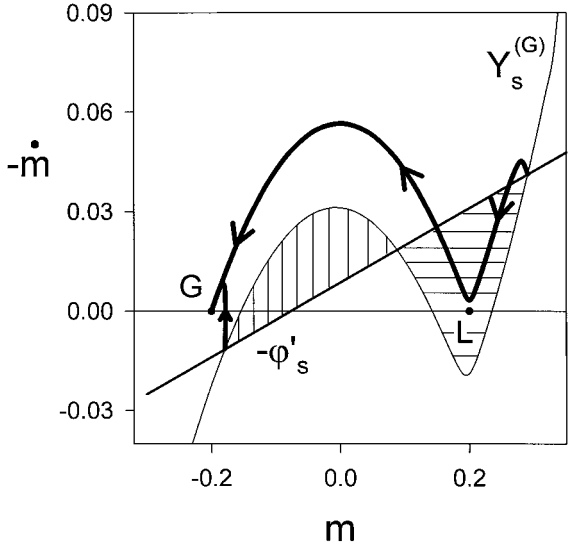

Fig. 3. Computed phase portrait for $a_3 = -0.05$ and $a_4 = 0.15$, corresponding to a long-range force which prevents complete wetting. The contact-potential curve $-\varphi'_s$ is chosen so that it intersects $Y_s^{(G)}$ thrice. The two outer intersections correspond to local minima of the free energy, which signify a thin film and a thick film. The associated trajectories are shown (thick lines with arrows). The area enclosed between $-\varphi'_s$ and $Y_s^{(G)}$ adds up to (approximately) zero, so that the two profiles represent two-phase coexistence of surface states. A critical wetting transition is possible, for $a_3 \to -0$, in the thick-film profile that starts at the outermost right intersection, with $m_1 \approx 0.3$. In contrast, in the limit $a_3 \to -0$ the thin film remains thin.

thin–thick phase transition occurs when the two hatched areas are equal. For fixed contact potential φ_s this can be achieved either by varying the temperature T or the long-range field amplitude(s).

The mechanism for critical wetting under long-range forces is, as mentioned before, the incipient degeneracy of $Y_s^{(G)}$ and $Y_s^{(L)}$, in the limit $a_3 \to 0$, with $a_3 < 0$ (antagonist). This degeneracy only occurs sufficiently far to the right (L-side) of the phase portrait, and can be best understood[22] by considering the artificial case $a_4 = 0$ for which the incipient phase portrait for $a_3 \to -0$ is just the standard short-range-forces portrait. However, to obtain the power-law divergence of the thickness of the wetting layer, it is necessary to assume $a_4 > 0$ (or, more generally, to include a positive term at some higher order). A long-range field which contains *only* the a_3/z^3 term leads to a logarithmic divergence of the layer thickness at critical wetting, resulting from the balance between exponentially

decaying repulsion and power-law attraction of the interface by the wall.[11] Our computations confirm this.

It is worth emphasizing that the vanishing of the leading amplitude a_3 is a necessary but not a sufficient condition for critical wetting to occur. Indeed, assuming that the long-range forces are weak (which we have implicitly done by considering the short-range analysis as a reasonable starting point for the physical system[5]), critical wetting can only occur for states which show *complete* wetting in the absence of long-range forces. These states are situated to the right of the liquid fixed point L. Since all those states are in principle candidates for critical wetting the precise location of the contact-potential curve $-\varphi_s'$ is unimportant, as long as it intersects $Y_s^{(G)}$ sufficiently far to the right in the phase portrait. Thus, given a situation of this type, the locus of critical wetting transitions is determined by the zeroes of the Hamaker constant as a function of temperature, alkane chain length, etc.

We remark that for long-range forces that oppose wetting, a first-order transition between a thin and a thick film replaces the first-order wetting transition which would occur if long-range forces are neglected. Consequently, provided the temperature of the first-order transition is (not too far) below that for which a_3 vanishes, the critical wetting transition is preceded by a thin–thick transition. This can give rise to an interplay between these two transitions, leading to *critical-endpoint* phase diagrams as predicted theoretically in wetting in fluids,[13, 23] and also in type-I superconductors.[7] A critical endpoint is the terminus where a line of critical wetting transitions ends as it meets a line of first-order surface transitions. At that point first-order thin–thick transitions change to first-order wetting transitions. This scenario clearly provides an interesting experimental challenge.

We now show that the wetting layer thickness l very close to the critical wetting transition, i.e., asymptotically for large l, obeys the simple relation

$$h(l) = 0 \tag{3.1}$$

Since h corresponds to the asymptotic part of the disjoining pressure Π, this relation expresses the vanishing of that pressure, which, depending on its sign, acts to thin or thicken the film. In general, $\Pi(l) = 0$ is a condition which the equilibrium layer thickness l must fulfill. Let us demonstrate (3.1), for example, for the choice $h(z) = a_3 z^{-3} + a_4 z^{-4}$, with $a_3 < 0$ and $a_4 > 0$. Since $a_3 < 0$ the surface free energy of a thick but finite wetting layer is *lower* than that of an infinitely thick one by an amount given by the interface potential $V(l)$, and we have

$$V(l) \approx 2m_0 \int_l^\infty dz\, h(z) \tag{3.2}$$

where $2m_0$ is the difference between liquid and gas densities in bulk. This result follows from (2.1) and the assumption that l is large enough so that an interface at l has nearly the same structure as an interface at infinity. After integration we obtain, for large l, the asymptotic form (1.2),

$$V(l) \approx Al^{-2} + Bl^{-3} \tag{3.3}$$

with $A = m_0 a_3$ and $B = 2m_0 a_4/3$. Now, since the equilibrium layer thickness is obtained by minimizing $V(l)$ with respect to l, we obtain (3.1). Consequently, in our example the layer thickness varies as

$$l \sim -a_4/a_3 \tag{3.4}$$

which diverges for $a_3 \to -0$. We have verified this asymptotic behavior in our computations.

Next we turn to the case $a_3 > 0$ (agonist), corresponding to the possibility of first-order wetting transitions. Figure 4 shows a computed phase portrait for $a_3 = 0.1$ and $a_4 = 0$, displaying an inverted golf club shape for $Y_s^{(G)}$. Besides the initial condition curves the figure shows the curve $-\varphi_s'$, which serves to locate the initial conditions of extremal profiles. We have again chosen this curve to be a straight line for simplicity, and have placed it so as to provide (nearly) equal areas, as indicated by the hatched regions. With this choice the system is close to a first-order phase transition between a thin film and an infinitely thick (macroscopic) wetting layer. The trajectories for both profiles are also shown (thick lines with arrows). Note that the macroscopic wetting layer consists of two parts. The first segment ends at L, and the second piece is a liquid-gas interface, from L to G. For the latter the long-range force plays no role, since only substrate–adsorbate long-range forces have been taken into account.

Before applying the theory to an actual system, we must reconsider the long-range field $h(z)$, of which in general only the *asymptotic* part for large z is known through the estimation (from experimental data or theoretical input) of the leading amplitudes a_3 and a_4. We must address the question whether it is appropriate to include the effect of $h(z)$ on the whole half-space $z > 1$, as is assumed in (2.1). This procedure would amount to employing $h(z)$ in a much larger region than where the asymptotic form is justified, and may lead to an overestimation of the contribution of the long-range forces. The investigation of this issue is taken up in the next Section.

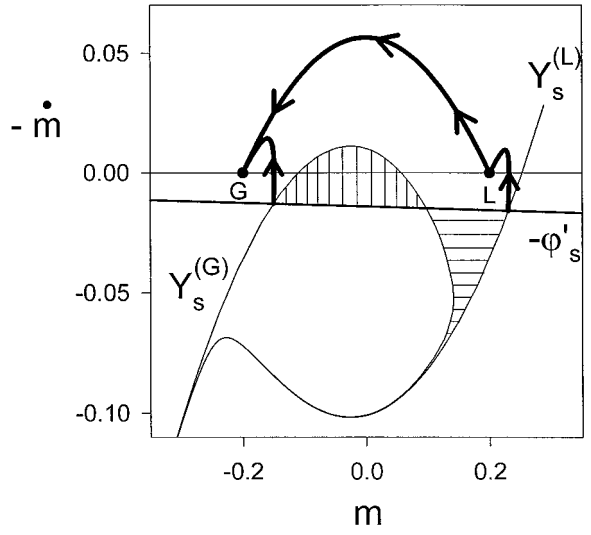

Fig. 4. Computed phase portrait for $a_3 = 0.1$ and $a_4 = 0$, corresponding to a long-range force that favours wetting. A first-order wetting transition occurs when the two hatched areas are equal. The trajectories associated with the coexisting thin film and macroscopic wetting layer are also shown (thick lines with arrows).

4. THE INTERFACE POTENTIAL $V(l)$ FOR LONG-RANGE FORCES

In this Section we first generalize the interface potential approach to systems with long-range forces. We then use $V(l)$ to determine the optimal threshold distance z^* at which the (asymptotic) long-range substrate–adsorbate field $h(z)$ is "switched on." The phenomenological parameter z^* provides a means of interpolating smoothly between a system with short-range forces only ($z^* = \infty$), and a system in which the long-range field $h(z)$, valid for large z, is added already from the substrate position onwards ($z^* = 1$).

Clearly, in order to obtain a realistic description of a specific system z^* should not be taken too close to the substrate, since the employed form of $h(z)$ is not appropriate there. On the other hand, z^* should not greatly exceed the particle diameter (given by the repulsive core of the pair potential), since the attractive tail of the interparticle interaction should be essentially incorporated correctly in the long-range forces. Thus, for self-consistency, z^* should be of the order of, but not smaller than, the microscopic particle size.

Although the introduction of the arbitrary parameter z^* is *a priori* a drawback, we shall show there exist meaningful criteria for fixing its value. One such option, which we adopt in this paper, is to require that the results from the theory be as insensitive as possible to the value of z^*. This corresponds to locating extrema of physical quantities as a function of z^*. We develop this criterion here, and apply it to the concrete example of pentane on water in the next Section.

The surface free-energy functional, with explicit dependence on the threshold distance z^*, reads

$$\bar{\gamma}[m; z^*] = \int_1^\infty dz \left\{ \frac{1}{2} \left(\frac{dm}{dz} \right)^2 + f(m(z)) \right\} - \int_{z^*}^\infty dz\, h(z)\, m(z) + \varphi_s(m_1) \qquad (4.1)$$

The application of the variational principle is now concerned with two intervals. On $[1, z^*]$ only short-range forces are involved and the profile obeys the equation of motion with $h(z) = 0$. On $[z^*, \infty]$ the long-range forces are included and the Euler-Lagrange equation is (2.4). At $z = z^*$ the profile and its first derivative are continuous but the second derivative makes a jump of magnitude $h(z^*)$. The boundary condition at $z = 1$ is given by (2.6) as before, and the bulk condition by (2.5).

To study the effect of changing z^* we may examine the modification of the phase portraits and trajectories, but a more powerful means of getting direct insight into the physical implications is to study the interface potential $V(l)$. As we stated before, this potential is an auxiliary free-energy function which estimates the free-energy cost associated with a wetting layer of presupposed thickness l. Thus, $V(l)$ gives the free energy of a *constrained* and therefore in general *non-equilibrium* profile. The extrema of $V(l)$ reproduce the stable (minima) and unstable (maxima) thermodynamic states. In fact, while only the local minima of $V(l)$ have direct physical significance, the overall structure of $V(l)$ is relevant to kinetic phenomena (activation over an energy barrier, nucleation, spinodal decomposition, etc.).[26] In contrast with the equilibrium free energy, the extension $V(l)$ is not uniquely defined. There exist various definitions and computational schemes in the literature,[24, 25] and recently a critical analysis of derivations of $V(l)$ has been given by Fisher and Jin.[24] The scheme developed by these authors will be implemented in our analysis and generalized to long-range forces.

We now outline the computation of $V(l)$. For concreteness we study a system in the vicinity of a first-order wetting transition, so that, typically, $V(l)$ displays two minima (thin film and thick wetting layer) and one maximum which governs the free-energy barrier between the two (meta-)stable states. Following Fisher and Jin we employ a local "crossing" constraint.

The wetting layer thickness l is imposed by forcing the profile $m(z)$ to cross a chosen value m^x at $z - z_s = l$, where $z_s = 1$ is the substrate location. Thus, in our coordinates the constraint reads

$$m(l+1) = m^x \tag{4.2}$$

The choice of m^x is fairly arbitrary (and can be exploited in a sophisticated way[27]), but we will adopt the simple point of view that m^x must be located within the interfacial region, i.e., $-m_0 < m^x < m_0$, and adhere to the obvious choice $m^x = 0$ practiced by Fisher and Jin. Application of the variational principle with this local constraint is straightforward, and has been described in detail for short-range forces.[24] The main peculiarity is that the constrained profiles naturally display a *discontinuous* first derivative at the matching point $z = l+1$, while all the usual conditions (including that at the boundary) apply on the intervals $[1, l+1]$ and $[l+1, \infty]$. If one wishes to smooth the singularity at the matching point, one can employ the recently proposed generalization of the crossing constraint,[28] but we do not pursue this here. Instead, we generalize the local crossing constraint to long-range forces, as follows. The function $V(l)$ generally consists of three segments, that we denote by A, B and C.

Segment A: $l > z^* - 1$

For a chosen value of m at the wall, $m_1 > 0$, the initial derivative is determined from the boundary condition $\dot{m}_1 = \varphi_s'(m_1)$. The equation of motion (2.4) with $h(z) = 0$ is then iterated until $z = z^*$. Subsequently, the full Eq. (2.4) is iterated starting from $m(z^*)$ and $\dot{m}(z^*)$, until $m = 0$ is crossed. At that junction $z = z^x$, and l is then obtained from the identification $l = z^x - 1$. Next, (2.4) is iterated starting from $m = 0$ and the derivative $\dot{m}(z^x)$ is *adjusted* so that the bulk condition $m \to m_b$ is fulfilled for $z \to \infty$. Note that, in general, this procedure yields a jump in $\dot{m}$ at the crossing point (cf. ref. 24). The constrained free energy $V(l)$ is obtained by computing (4.1) along with the trajectory. The magnitude of the jump goes to zero whenever the trajectory coincides with one that extremizes the free energy (4.1) *without* constraint. Such coincidence occurs precisely at the extrema of $V(l)$.

Segment B: $0 < l < z^* - 1$

For a chosen wall value $m_1 > 0$, the initial derivative is determined from the boundary condition $\dot{m}_1 = \varphi_s'(m_1)$. The equation of motion (2.4) with $h(z) = 0$ is then iterated until $m = 0$ is crossed. At that junction $z = z^x$

and l is then obtained from the identification $l = z^x - 1$. Next, (2.4) is iterated starting from $m = 0$ and a trial value for the derivative, until $z = z^*$. Subsequently, (2.4) is iterated again starting from $m(z^*)$ and $\dot{m}(z^*)$, and the previously chosen trial value $\dot{m}(z^x)$ must be adjusted so that the bulk condition $m \to m_b$ is fulfilled for $z \to \infty$.

Segment C: $l < 0$

Negative values of l are possible and meaningful, since in general l is not the physical thickness of the wetting film, but a mathematical intercept which may lie "behind" the substrate. If the adsorption is small, the order parameter at the wall barely exceeds the vapour density, leading to $l < 0$. In such cases there is, strictly speaking, no wetting film.

For this segment, which pertains to the *thin-film* regime, the procedure of the crossing constraint is impracticable, simply because the profile does not cross m^x. To remedy this it suffices to lower m^x for most applications so that even for small adsorption $l > 0$ (as we shall illustrate in the next Section). However, even if m^x is lowered in value, there is always a point where the crossing criterion ceases to apply, as the adsorption or "coverage" contained in the profile is reduced below a certain amount. To complete the calculation of the interface potential nevertheless, one must have recourse to an alternate procedure in this low-coverage regime. We turn to the earlier method of Lipowsky *et al.* and Brezin *et al.*,[25] which amounts to computing the interface potential by imposing the constraint of *fixed wall value* m_1. The difference with respect to the Fisher–Jin approach is that the usual wall-boundary condition is no longer in effect (since m_1 is fixed). Furthermore, the profile $m(z)$ is everywhere smooth. The thin-film equilibrium state is reproduced as the minimum of the interface potential. The connection between the segments $l < 0$ and $l > 0$ of $V(l)$ is smooth (the weak singularity at $l = 0$ is imperceptible).

The definition of l in the case $l < 0$ is possible as follows. For a chosen wall value $-m_0 < m_1 < m_0$,[29] the profile is imagined to have a virtual extension into the substrate, which can be traced by iterating backwards from $z = 1$ to lower z. Of course, this virtual profile obeys the short-range equation of motion, since $z^* \geqslant 1$ in any case. The explicit solution is well known.[25] It is a shifted tanh-profile,

$$m(z) = -m_0 \tanh\left[\sqrt{2}\,(z - \delta)\, m_0\right] \tag{4.3}$$

where the shift δ is related to the wall value through

$$m_1 = -m_0 \tanh\left[\sqrt{2}\,(1 - \delta)\, m_0\right] \tag{4.4}$$

so that $\delta < 1$ for $m_1 < 0$. Note that this virtual profile crosses $m = 0$ at $z = \delta$, so that a sensible definition of l is

$$l = \delta - 1 \tag{4.5}$$

Iteration of the profile and computation of $V(l)$ can be done as follows. Start from a chosen l and correspondingly, set $z = l + 1$. Take $m = 0$ and choose a trial value for the derivative $\dot{m}(l+1)$. Iterate the equations for short-range forces until $z = 1$ is reached. At that point the free-energy computation is started (since the virtual part of the profile does not contribute to the free energy). The remainder of the profile is obtained by iterating the equations for short-range forces until $z = z^*$ and the long-range forces are switched on starting from that distance. Finally the initial trial derivative must be adjusted so that the bulk condition is satisfied. The result is that the profile and its first derivative are continuous everywhere (including in the virtual part).

The resulting interface potential $V(l)$ is illustrated in Fig. 5, for various choices of z^*. The system parameters are taken to correspond to a first-order wetting transition in the limit of short-range forces (i.e., for $z^* = \infty$).

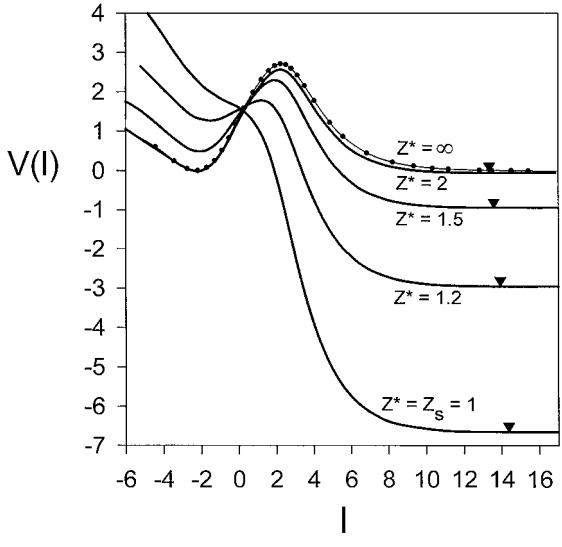

Fig. 5. Interface potentials $V(l)$ versus wetting layer thickness l, for threshold distances $z^* = 1$, 1.2, 1.5, 2, and ∞. The system parameters are tuned to a first-order wetting transition in the absence of long-range forces, i.e., for $z^* = \infty$ (thin line with dots). The triangles indicate the minima of $V(l)$ corresponding to the wetting layer.

Assuming the simplest form for the short-range contact energy $\varphi_s(m_1) = -h_1 m_1$, this requirement is met for $h_1 = 0.68125 c m_0^2$, with $c = \sqrt{2}$ and $m_0 = 0.2$ in our units. As far as the long-range field is concerned, we take the same parameters as in the system described in Fig. 3, $a_3 = -0.05$ and $a_4 = 0.15$. As expected the interface potential for short-range forces displays two equal minima, one at $l < 0$ (thin film) and the other at $l = \infty$ (macroscopic wetting layer).

Adding the long-range forces at maximal strength ($z^* = 1$), while keeping all other parameters fixed, completely distorts the free-energy balance in favour of the wetting layer. In fact, the thin-film minimum is lifted and removed, as the system is driven beyond the spinodal[31] of the thin-film state. The thick-film state is absolutely stable, but the thickness of the wetting layer (indicated by the triangles) is reduced from macroscopic to finite ($l \approx 14$) due to the antagonistic long-range force at large z ($a_3 < 0$). Thus, the effect of the long-range field is twofold: the free-energy balance is distorted and the wetting layer acquires a finite thickness. However, these two important effects are largely *independent* of one another. Indeed, as soon as z^* is increased slightly, from $z^* = 1$ to 1.5, the free-energy balance associated with the short-range forces is already almost restored, while the thickness of the wetting layer remains at $l \approx 14$. Further increasing z^* to 2

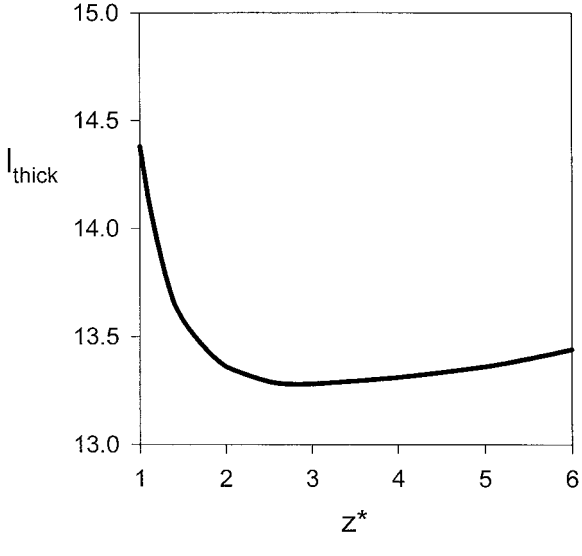

Fig. 6. Thickness l_{thick} of the equilibrium thick film, as a function of the threshold distance z^* for the onset of the long-range field $h(z)$. The triangles in Fig. 5 correspond to points on this curve.

is sufficient to restore the interface potential minimum for the thin film completely, while again the thick layer is unaffected.

These results suggest that z^* can be chosen such that

(i) The properties of the thick film, in particular its thickness, are determined by the long-range forces.

(ii) The properties of the thin film, in particular its thickness, are not modified by the inclusion of the long-range forces. These properties can be fully incorporated in the short-range Cahn–Landau model, by appropriately tuning the contact potential φ_s.

(iii) The long-range forces do not (or only slightly) modify the free energy balance between the thin and the thick film. In other words, they do not appreciably change the difference $V(l_{\text{thin}}) - V(l_{\text{thick}})$. Note that in the absence of long-range forces (such that $l_{\text{thick}} \to \infty$) this difference is the spreading coefficient S.

In order to examine quantitatively how these criteria can be met, we have plotted in Fig. 6 the thickness of the thick film as a function of z^*, and in Fig. 7 the thickness of the thin film. Clearly, for the preservation of the thick film z^* may not be taken too large, since necessarily $l_{\text{thick}} \to \infty$ for $z^* \to \infty$. The optimal choice seems to be $z^* \in [2, 4]$, the interval where l_{thick} is least sensitive to z^*. From the point of view of the thin film it

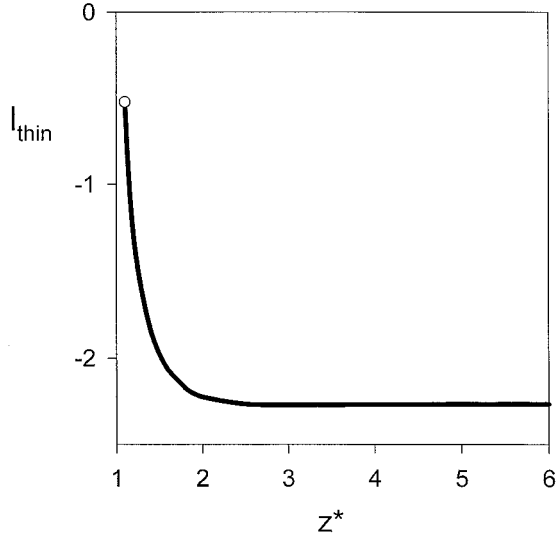

Fig. 7. Thickness l_{thin} of the metastable thin film, as a function of the threshold distance z^* for the onset of the long-range field $h(z)$. The open circle near $z^* = 1.1$ marks the surface spinodal, at which the thin film state becomes unstable.

suffices to take $z^* > 2$ to meet the proposed objective. In conclusion, the two physical requirements for a perturbation theory based on weak long-range forces are compatible, and lead to a choice of z^* only slightly greater than the wall position (at a microscopic distance away from it). In practice it suffices to fix z^* at the point where, coming from small z^*, the thin-film characteristics have converged. We recall that this is not the only possible criterion for fixing z^*, but it is the appropriate one if we assume that the effect of the long-range forces is only a weak perturbation of the free energy.

After these basic notions and elementary examples, we turn to a specific application to alkanes on water. As far as the short-range forces are concerned the phase portrait analysis has been worked out in ref. 5. We will not repeat this here, but proceed directly to include the long-range forces in the perturbative spirit developed so far.

5. APPLICATION TO PENTANE ON WATER

In this Section we extend the preliminary study of possible wetting transitions of pentane on water[5] by taking into account the van der Waals forces in the Cahn–Landau theory as described in the foregoing Sections. A brief summary of the calculations was presented in ref. 4, where the experimental discovery of a critical wetting transition of pentane on water was reported. It is our purpose here to give a complete account of the theory.

With pentane at liquid–vapour coexistence playing the role of the adsorbate and water that of the substrate, the surface free-energy functional reads

$$\bar{\gamma}[C] = \phi_s(C_s) + \int_0^\infty dZ \left\{ \frac{m}{2} \left(\frac{dC}{dZ} \right)^2 + \Delta f(C, C_G) \right\} - \int_\zeta^\infty dZ\, H(Z)\, C(Z) \tag{5.1}$$

Here $C(Z)$ denotes the local density of pentane. The water phase is an inert spectator phase which occupies the half-space $Z < 0$. For $Z > 0$ we assume pure pentane at liquid–vapour coexistence. The value C_s is the surface density of pentane, $C_s = C\ (Z = 0)$. The parameter m is the so-called influence parameter[5] (not to be confused with the density variable of the previous Sections). The contact energy ϕ_s pertains to the short-range part of the forces and was studied and determined previously for this system.[5] The "effective" free energy per unit volume, Δf, is given by

$$\Delta f(C, C_G) \equiv f(C) - f(C_G) - (C - C_G) \left. \frac{df}{dC} \right|_{C_G} \tag{5.2}$$

where f is the bulk Helmholtz free-energy density (with the shape of an asymmetric double well). The reference density C_G is that of the bulk gas phase. Full expressions for the free-energy density f, the pressure p and the chemical potential μ have been given in ref. 5. The new addition with respect to the previous work is the long-range field $H(Z)$ originating from the van der Waals forces. The cut-off distance ζ must be determined self-consistently and plays the role of the threshold distance z^* of the previous Section.

It is useful to make all the quantities dimensionless, so that we can work with a reduced free-energy $\bar{\gamma}[c]$ which is a functional of the reduced density profile $c(z) \equiv bC(Z)$, where b is the excluded volume of a particle.[5] Consequently, $0 \leqslant c \leqslant 1$. A reduced free-energy density is obtained as f/P_c, with P_c the critical pressure of pentane. Scaling the variables we naturally arrive at the definition of a new physical length scale λ, through

$$\lambda^2 \equiv \frac{m}{b^2 P_c} \tag{5.3}$$

Using the parameter values given in ref. 5, we arrive at the estimate $\lambda \approx 32.3$ Å. This is a microscopic length, but significantly larger than the size (diameter) of the pentane molecule, which is about 6 Å. The reduced free energy $\bar{\gamma}[c] \equiv \bar{\gamma}[C]/\lambda P_c$ reads

$$\bar{\gamma}[c] = \frac{\phi_s(c_s)}{\lambda P_c} + \int_0^\infty dz \left\{ \frac{1}{2}\left(\frac{dc}{dz}\right)^2 + \Delta f(c, c_G)/P_c \right\} - \int_{z^*}^\infty dz\, H(z)\, c(z)/bP_c \tag{5.4}$$

with $z^* \equiv \zeta/\lambda$.

In order to identify the amplitudes of the long-range field and to relate them to the Hamaker constant[4] we express the reduced free-energy difference between the state with a liquid-vapour interface at a distance l from the water surface and the state with an interface at an infinite (macroscopic) distance as follows,

$$V(l) - V(\infty) = \int_l^\infty dz\, H(z)(c_L - c_G)/bP_c = A/l^2 + B/l^3 \tag{5.5}$$

Clearly, $V(l)$ is the interface potential defined and discussed in the previous Section and l is a dimensionless length which gives the wetting layer thickness in units of λ. As commonly done, we take $V(\infty) = 0$. The densities c_L and c_G correspond to bulk liquid and vapour, respectively. If we define a reduced long-range field through $h(z) = a_3/z^3 + a_4/z^4 \equiv H(z)/bP_c$, we obtain, assuming $c_G \ll c_L$, the relations $A = c_L a_3/2$ and $B = c_L a_4/3$.

We now proceed to determine typical magnitudes of a_3 and a_4. The Hamaker constant W is related to A through[4]

$$A\lambda P_c = -W/12\pi \tag{5.6}$$

Using the available estimates of W and of the next-to-leading term in the expansion of the interface potential in inverse powers of l,[2, 32] we find at about $T = 30°\text{C}$, $a_3 \approx -6 \times 10^{-4}$ and $a_4 \approx 1.5 \times 10^{-3}$. Since $a_3 < 0$ we are dealing with the antagonist case, so that thick wetting layers cannot form. It should be stressed that a_3 has an important temperature dependence, while a_4 does not. The leading amplitude a_3 decreases in magnitude with increasing T and passes through zero at about $T = 53°\text{C}$, the critical wetting point.[2] As discussed previously, the mechanism for the wetting transition is the divergence of the film thickness in the limit $a_3 \to -0$.

We are now ready to apply the theoretical tools developed in the previous Sections, and begin with the analysis of the phase portrait.

5.1. Phase Portrait Including Long-Range Forces

The analysis given in Section 2 allows one to incorporate the effect of the long-range field starting from the preliminary phase-portrait analysis reported in ref. 5. Note that the substrate (i.e. water) is located at $z = 0$ instead of $z = 1$, and that, unlike $f(m)$ in the standard model, the free energy density $f(c)$ does not have a special symmetry.

If we choose the threshold distance z^* for the onset of the long-range field not too small (e.g., $z^* = 0.2$, a choice which will be justified below), we are in the "perturbative" regime and the global phase portrait is quite similar to that with short-range forces alone. Figure 8 illustrates this. The temperature has been set to the value $T = -30°\text{C}$, for which the simple Cahn theory predicts a first-order wetting transition.[5] The amplitudes of the long-range field have been fixed at $a_3 = -0.003$ and $a_4 = 0.001$, which have the correct sign and order of magnitude for the system at this temperature.

In Fig. 8 we have plotted the curve of initial conditions $-(dc/dz)_s$ versus c_s, for trajectories that eventually reach the fixed point G (with $c_G = 0.00023$). This curve is denoted by $Y_s^{(G)}$. On the other hand, the contact-energy curve $-(d\phi_s/dc)/\lambda P_c$ is given in ref. 5. For this temperature and in the relevant density range this curve is well approximated by a straight line, $h_1 + gc$, where h_1 is the reduced "surface field" and g the reduced "surface coupling enhancement." The intersections of the two curves correspond to initial conditions with extremal free energy.

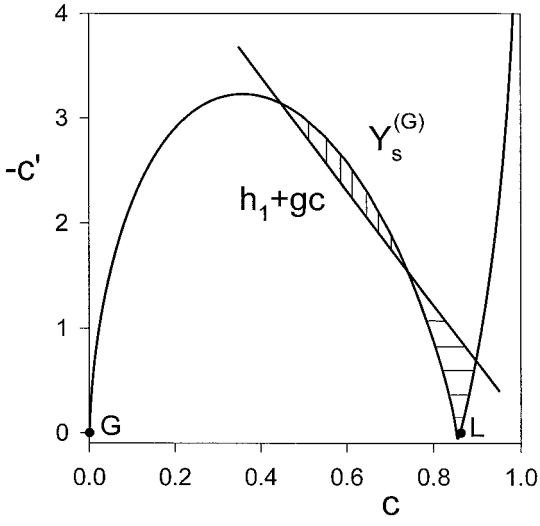

Fig. 8. Phase portrait for pentane on water including the effect of the long-range forces, for $T = -30°C$. Plotted is the curve $Y_s^{(G)}$ of "velocity" $-c' \equiv -dc/dz$ versus "position" c, corresponding to initial conditions that eventually reach the fixed point G. Also shown is a linear approximation to the contact-energy curve, which intersects $Y_s^{(G)}$ thrice. The outermost intersections correspond to initial conditions for the thin film (left) and the thick wetting layer (right). The system is at a first-order thin–thick phase transition when the two hatched areas are equal.

Note the similarity between our Fig. 8 and Fig. 6 of ref. 5 on a global scale. However in the vicinity of the liquid fixed point L the antagonistic long-range field manifests itself clearly and complex structure becomes apparent on a smaller scale, as shown in Fig. 9. We distinguish two main lines. These correspond to the *initial condition* curve $Y_s^{(G)}$, and to a typical *trajectory* (thick line with arrows). This trajectory starts on $Y_s^{(G)}$ at $c(0) = 0.91$ and consists of two segments which are continuously connected at $z = z^* = 0.2$, with $c(z^*) = 0.858$ (open circle), where d^2c/dz^2 makes a jump. For $z < z^*$ the equations with $h(z) = 0$ apply, while for $z > z^*$ the long-range field is taken into account.

For comparison, we have also drawn the phase-portrait curve for short-range forces (dashed lines meeting at L) found in ref. 5. The initial-condition curve as well as all trajectories converge towards and become part of the dashed lines in the limit $z^* \to \infty$. The contact-potential curve (see Fig. 8) has been omitted in Fig. 9. The equation defining the phase-portrait for short-range forces is, in our reduced variables,

$$|dc/dz| = \sqrt{2\Delta f(c)/P_c} \tag{5.7}$$

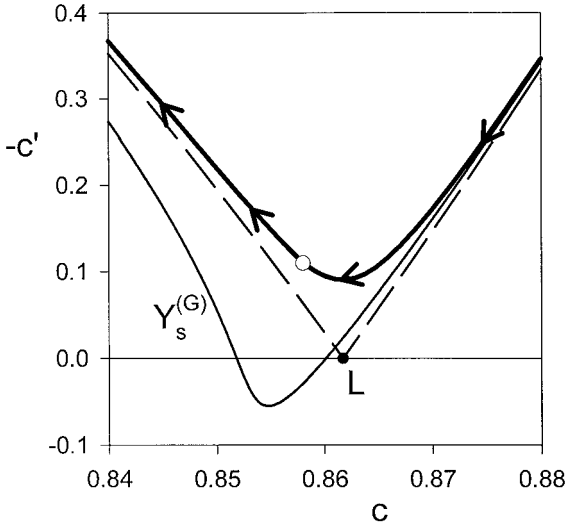

Fig. 9. Detail of the phase portrait for pentane on water (Fig. 8) in the vicinity of the bulk liquid point L. Shown are the initial-condition curve $Y_s^{(G)}$ (solid line), a trajectory for a thick wetting layer (thick line with arrows), and the phase portrait for short-range forces (dashed lines). The open circle on the trajectory marks the point where $z = z^*$.

Note that Fig. 6 of ref. 5 employs the original energy and density variables.

As far as the initial-condition curve and the trajectories are concerned the physical situation is similar to that in Fig. 3 for the standard model (see also Fig. 4 in ref. 2). From the phase portrait we conclude that all wetting layers are of finite rather than macroscopic thickness, since trajectories starting to the right of L (with $c_L = 0.862$) and eventually reaching G pass by L in a finite "time" z. We now proceed to the justification of our choice $z^* = 0.2$.

5.2. The Short-Distance Cutoff z^* for the Long-Range Field $h(z)$

We study how the thicknesses of the thin and the thick film depend on the threshold distance z^*, for system parameters which correspond to the vicinity of a first-order wetting transition when only short-range forces are taken into account. Recall that short-range forces are reproduced in the limit $z^* \to \infty$. In that limit the thickness of the thick film diverges, so that complete wetting results.

In order to define the thickness l of an adsorbed pentane film, we choose the point in the pentane liquid–vapour interface where the density

(in reduced units) equals 0.1, so that $c(l) \equiv 0.1$ defines l implicitly. Note that this density corresponds to about $100 \times c_G$ and about $0.1 \times c_L$. The choice of this density is arbitrary, as long as it is intermediate between the liquid and gas densities. The thickness l undergoes only a small shift under a change of definition, because the liquid-gas interface is fairly sharp on the molecular scale. For example, changing the "midpoint" density $c(l)$ from 0.1 to 0.35 (which corresponds to the average of the densities of liquid and gas) leads to a decrease in l of 0.09, equivalent to 2.8 Å.

Thin Film. We take $T = -30°C$ as before and examine l_{thin} for a variety of choices of the amplitudes a_3 and a_4. As proposed in Section 4 we determine the optimal z^* by requiring that l_{thin} remains constant upon further increase of z^*. For $a_3 = -0.0006$ and $a_4 = 0.001$ this leads to $z^* = 0.18$, which corresponds to a physical distance of 5.8 Å. If we increase a_3 in magnitude to a more appropriate value $a_3 = -0.003$ for the low temperature under consideration, the change in z^* is imperceptible, so that $z^* = 0.18$ is robust. Increasing the magnitude of a_3 further to -0.006 leads to a small decrease of z^* to 0.14. The plot of l_{thin} versus z^* for this case is shown in Fig. 10. If we double a_4 to 0.002, and reset $a_3 = -0.003$, the change in z^* is again small, from 0.18 to 0.19. Further increasing a_4 to 0.005 results in $z^* = 0.21$, a value which persists for a_4 as high as 0.01.

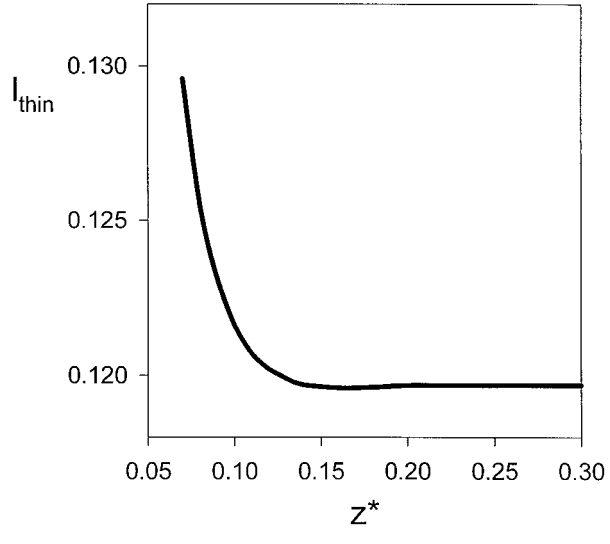

Fig. 10. Typical plot of the thickness l_{thin} of the metastable thin film of pentane, as a function of the threshold distance z^* for the onset of the long-range field. The parameter values are $a_3 = -0.006$ and $a_4 = 0.001$.

We conclude that the optimal z^* can confidently be taken to be 0.2, so that the cut-off turns out to be about the size of a pentane molecule. This is certainly a reasonable result.

Thick Film. For consistency the optimal value of z^* determined from the foregoing analysis of l_{thin} should not be far from the z^* value which minimizes l_{thick} (as proposed in Section 4). Let us verify this. For the case $a_3 = -0.006$ and $a_4 = 0.001$ the plot of l_{thick} versus z^* is shown in Fig. 11. We conclude that l_{thick} is minimal for $z^* \approx 0.17$. This is only slightly larger than the optimal value $z^* = 0.14$ found from the thin-film analysis for the same long-range field amplitudes (see Fig. 10). A bigger difference is found for $a_3 = -0.003$ and $a_4 = 0.001$, in which case l_{thick} is least sensitive to the cut-off for $z^* \approx 0.33$, while the thin film properties have converged already for $z^* > 0.18$. Even in this case, $z^* = 0.33$ corresponds to only 11 Å and is still of the order of the molecular size.

To elucidate further the role of z^* we proceed, as indicated in Section 4, to study the interface potential.

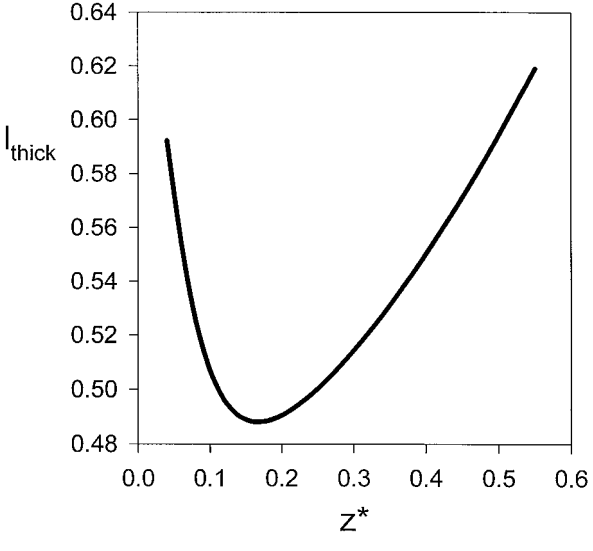

Fig. 11. Typical plot of the thickness l_{thick} of the equilibrium thick film of pentane, as a function of the threshold distance z^* for the onset of the long-range field. The parameter values are $a_3 = -0.006$ and $a_4 = 0.001$.

5.3. The Interface Potential $V(l)$ for Pentane on Water

Here we study density profiles $c(z)$ for $T=-30°C$ and long-range field amplitudes $a_3=-0.00216$ and $a_4=0.00130$. These amplitudes have been calculated based on the available experimental results summarized in ref. 2 and given in more detail in ref. 32. The presumed temperature dependence of a_3 will be given below, when we discuss critical wetting. The density profiles are subject to the constraint of fixed l. That is, they satisfy the boundary condition $c'(0)=-h_1-gc(0)$ at the water surface and the crossing constraint $c(l)=0.1$. The cases $l>z^*$ and $0<l<z^*$, referred to as segments A and B in the previous Section, are relevant to our present application (recalling that z^*-1 of the previous Section is to be replaced by z^* because the "wall" is now at $z=0$). Note that, due to the choice of the fairly low crossing density $c(l)=0.1$ we are not concerned with Segment C ($l<0$). Indeed, even the thin film state has a surface density well in excess of 0.1 so that $l>0$ is guaranteed for all relevant density profiles.

The contact-energy parameters h_1 and g have been determined in close accord with the results put forward in ref. 5 for the model with short-range

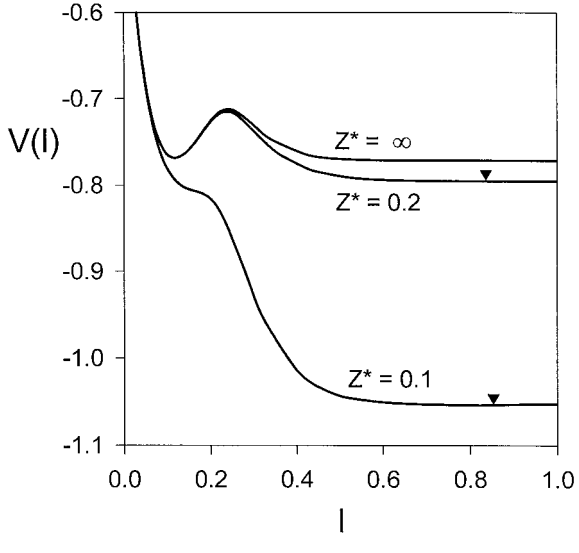

Fig. 12. Interface potentials $V(l)$ versus wetting layer thickness l for pentane on water, and for threshold distances $z^*=0.1$, 0.2, and ∞. The triangles indicate the minima of $V(l)$ corresponding to the thick film. The film thicknesses are $l=0.837$ for $z^*=0.2$ and $l=0.853$ for $z^*=0.1$. The system parameters are tuned to a first-order wetting transition in the limit of short-range forces ($z^*=\infty$). The long-range field is chosen slightly differently than in the preceding figures 10 and 11 (see text).

forces. The values presently employed are $h_1 = 5.58$ and $g = -5.451$. This leads to surface densities $c(0) \approx 0.45$ and $c(0) \approx 0.90$ for the thin and the thick film, respectively. The reduced free energy computed using (5.4) for profiles that satisfy the crossing constraint is, without further normalization or shift, presented as $V(l)$ in Fig. 12 for three choices of the long-range field cut-off z^*.

As has already been anticipated, the potential for $z^* = 0.2$ displays characteristics similar to the short-range potential found for $z^* = \infty$. In fact, the potential follows the short-range limit closely up till $l = \mathcal{O}(z^*)$. This is because constraining the interface to a distance l closer than z^* from the water surface leads to a negligible influence of the long-range forces on the density profile (the trajectory). The difference between the cases $z^* = 0.2$ and $z^* = \infty$ thus lies in the tail of the potential, which for $z^* = 0.2$ is of power-law character (with the thick-film minimum at about $l = 0.84$), while the short-range potential decays exponentially to its minimum at $l = \infty$.

On the other hand, if z^* is decreased to 0.1, important distortion of $V(l)$ occurs both at small and large l. The free-energy balance between the thin and the thick film is disrupted, and in fact, the system is already pushed across the spinodal of the thin film. Only the thick film (with slightly modified thickness $l \approx 0.85$) is thermodynamically stable. We conclude once more that $z^* = 0.2$ is an appropriate cut-off for incorporating the long-range forces in a perturbative spirit, without changing much the free-energy landscape dictated by the short-range potential.

Finally we turn to the phenomenon of greatest recent interest in this system, the critical wetting transition at 53°C.

5.4. Wetting Layer Thickness Approaching Critical Wetting

The main feature of the system under study relevant to critical wetting is the vanishing of the Hamaker constant at about 53°C.[2] In our reduced variables this entails the following variation of a_3,

$$a_3 \approx u(T - T_w)/T_c \tag{5.8}$$

with $T_c = 469$ K and $T_w/T_c = 0.692$ for the critical wetting transition. The experimental data and a simple model calculation[2] indicate that a linear temperature dependence of the Hamaker constant is a reasonable approximation in a fairly wide temperature interval below T_w. We infer $u \approx 0.01047/c_L$. Note that the inverse dependence of a_3 on c_L follows from (5.5) and (5.6). Since c_L depends only weakly on temperature, varying between 0.86

at $T = -30°C$ and 0.76 at $T = 52°C$, a_3 depends almost linearly on T. Furthermore, assuming a_4 depends on T only through c_L we estimate

$$a_4 \approx 0.00112/c_L \tag{5.9}$$

Employing these amplitudes for the long-range field together with the previously derived amplitudes for the contact energy, and choosing the optimal cut-off as $z^* = 0.2$, we arrive at the equilibrium wetting layer thickness versus temperature presented in Fig. 13. The determination of the layer thickness close to T_w is difficult numerically (in spite of the use of quadruple precision), but the expected power law

$$l \propto (T_w - T)^{-1} \tag{5.10}$$

is clearly displayed by the points closest to T_w. As a guide to the eye a straight line with slope -1 is drawn besides the data. This line represents the simple asymptotic behavior (3.4), $l = -a_4/a_3$. The thicknesses that we

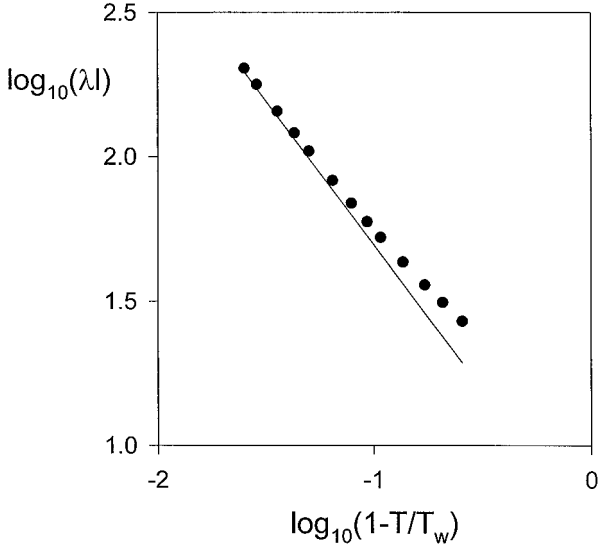

Fig. 13. Thickness of the wetting layer of pentane on water versus temperature, approaching the critical wetting transition. The actual thickness λl is in units of Å. The straight line is an asymptote to the data, obtained from a simple approximation for large l. The thicknesses agree qualitatively with the experimental results.[2] The power-law behavior (with exponent -1) is clearly seen. We remark that there is a uniform shift along the temperature axis with respect to the experimental log–log graph presented in ref. 2, where in the expression $1 - T/T_w$, temperature was expressed in degrees Celsius instead of Kelvin.

find in this way agree reasonably with the experimentally measured values. This is of course not a surprise, since the model parameters have been tuned to reproduce the experimental data at least in as far as the order of magnitude is concerned. Thus we obtain $l = 60$ Å at $T = 23°C$, $l = 83$ Å at $T = 32°C$, $l = 144$ Å at $T = 41°C$, and the last data point corresponds to $l = 203$ Å at $T = 45°C$. Note that this is still 8 K below T_w. The fact that the asymptotic behavior sets in quite early is due to the neglect of higher-order terms in the long-range field. This feature is of course not shared by the experimental data,[2] which fit reasonably well to an exponent -1, but with an error margin of about 0.3.[33]

6. CONCLUSIONS

A first attempt to predict the wetting behavior of linear alkanes on water using a Cahn-type theory was partially successful.[5] Reasonable agreement with experimental observations was obtained, except for pentane. The case of pentane is special in that a critical wetting transition was found experimentally,[2] which was not anticipated in the first theoretical description. This paradox was soon resolved by noting that the mechanism for the critical wetting transition is the change of sign, as a function of temperature, of the Hamaker constant which incorporates the net van der Waals interaction between the water-pentane and pentane-pentane interfaces.[2] The Cahn theory employed initially was restricted to systems with short-range forces and consequently missed this point.

Here we have developed in detail the adaptation of the Cahn theory to systems with van der Waals forces, and especially its application to pentane on water. The new theoretical aspects elaborated it this work are:

(i) The calculation and systematic use of phase portraits in a system with long-range forces. Due to the presence of these interactions the dynamical equation of motion is not integrable. This has led us to discuss the phase equilibria by examining the initial condition curves instead of the trajectories.

(ii) The calculation of the interface potential $V(l)$ in a system with long-range forces. We have provided a systematic derivation of $V(l)$ using a self-consistent scheme based on an extension of the Fisher–Jin crossing constraint to systems with long-range forces.

(iii) The introduction and optimization of a short-distance cut-off z^* for the long-range forces. We have optimized this parameter by requiring that the effect of the long-range forces be perturbative. This means that the relevant effects of the long-range forces (such as the inhibition of complete

wetting) remain present, but without modifying the characteristics of the thin-film state. This optimization criterion is not the only possible one, but we have shown that it is self-consistent. Indeed, we have obtained a physically reasonable *microscopic* z^*, slightly larger than the molecular size, for which the criterion is satisfied. Other criteria are, however, conceivable. For example, the parameter z^* can perhaps be fine-tuned to adjust the theory to new experimental results, such as the location of the first-order thin-thick transition in hexane on brine.[3]

Treating the long-range forces as a perturbation, as we have done in the present work, leads us to conclude that critical wetting is predicted for systems with antagonistic long-range forces at the temperature T_w where the Hamaker constant changes sign. Furthermore, a necessary condition for critical wetting is that the standard theory (with only short-range forces) should predict complete wetting around this temperature T_w. Indeed, only in that case will the wetting layer thickness diverge continuously, as the leading amplitude of the long-range field vanishes. Moreover, critical wetting is preceded by a first-order thin-thick transition whenever the short-range theory predicts a first-order wetting transition at a temperature $T_1 < T_w$. This is the case for several of the alkanes, albeit that for pentane the predicted first-order transition is below the freezing point of the substrate (the water phase) and is therefore inaccessible. For hexane on brine, it has been observed.[3]

In future work the interplay of the first-order thin-thick transition and the critical wetting transition is to be investigated further. The phenomenological Cahn–Landau theory is expected to be useful also in more complicated situations, such as in the presence of chemical and geometrical disorder, relevant to petroleum reservoirs. Indeed, the contact energy, the long-range field and the cut-off distance can be adapted, and the calculations can be carried out for curved substrates.[34]

Finally, we note that the theory we have employed is of mean-field type. This is justified in fluids with van der Waals forces, since the upper critical dimension above which mean-field theory can be trusted (in as far as the singularities at wetting phase transitions are concerned) is less than the physical dimension $d = 3$.[11]

ACKNOWLEDGMENTS

This paper is dedicated to John Cahn on the occasion of his 70th birthday. It is with pleasure and deep gratitude that J. O. I. recalls several stimulating and friendly discussions with John Cahn about wetting phenomena. We thank Chris Boulter, Ralf Blossey and Francis Clarysse for

a critical reading of the manuscript. J. O. I. is a Research Director of the Fund for Scientific Research of Flanders, and has been supported in part by the Belgian Concerted Action Programme (GOA) and Interuniversity Poles of Attraction Programme (IUAP). K. R. has been supported in part by the Wetenschappelijke Onderzoeksgemeenschap (WOG) during a visit to K.U.Leuven. LPS de l'ENS is URA 1306 du CNRS, associée aux universités Paris 6 et Paris 7. This research has been supported in part by the Flemish Government (Project VIS/97/01), contract Joule JOF3-CT95-0013, and the European Community TMR Research Network, Contract Nr. FMRX-CT98-0171.

REFERENCES

1. J. W. Cahn, *J. Chem. Phys.* **66**:3667 (1977).
2. K. Ragil, J. Meunier, D. Broseta, J. O. Indekeu, and D. Bonn, *Phys. Rev. Lett.* **77**:1532 (1996).
3. N. Shahidzadeh, D. Bonn, K. Ragil, D. Broseta, and J. Meunier, *Phys. Rev. Lett.* **80**:3992 (1998).
4. K. Ragil, D. Bonn, D. Broseta, J. O. Indekeu, F. Kalaydjian, and J. Meunier, *J. Petroleum Sci. Eng.* **20**:177 (1998).
5. K. Ragil, D. Bonn, D. Broseta, and J. Meunier, *J. Chem. Phys.* **105**:5160 (1996).
6. J. O. Indekeu, P. J. Upton, and J. M. Yeomans, *Phys. Rev. Lett.* **61**:2221 (1988); P. J. Upton, J. O. Indekeu, and J. M. Yeomans, *Phys. Rev. B* **40**:666 (1989).
7. J. O. Indekeu and J. M. J. van Leeuwen, *Phys. Rev. Lett.* **75**:1618 (1995); *Physica C* **251**:290 (1995).
8. See, e.g., P.-G. de Gennes, *J. Phys. Lett.* (France) **42**:L377 (1981); for background, see, e.g., B. V. Derjaguin, N. V. Churaev, and V. M. Muller, in *Surface Forces*, J. A. Kitchener, ed. (Consultants Bureau, New York, 1987).
9. P.-G. de Gennes, *C.R. Acad. Sc. Paris* **297**:II-9 (1983).
10. M. P. Nightingale, W. F. Saam, and M. Schick, *Phys. Rev. Lett.* **51**:1275 (1983); *Phys. Rev. B* **30**:3830 (1984).
11. R. Lipowsky, *Phys. Rev. Lett.* **52**:1429 (1984); *Z. Physik B* **55**:345 (1984); R. Lipowsky and D. M. Kroll, *Phys. Rev. Lett.* **52**:2303 (1984).
12. V. Privman, *J. Chem. Phys.* **81**:2463 (1984).
13. S. Dietrich and M. Schick, *Phys. Rev. B* **31**:4718 (1985); *Phys. Rev. B* **33**:4952 (1986).
14. C. Ebner, W. F. Saam, and A. K. Sen, *Phys. Rev. B* **31**:6134 (1985); *Phys. Rev. B* **32**:1558 (1985).
15. M. P. Nightingale and J. O. Indekeu, *Phys. Rev. B* **32**:3364 (1985).
16. C. Ebner and W. F. Saam, *Phys. Rev. Lett.* **58**:587 (1987); *Phys. Rev. B* **35**:1822 (1987); **37**:5252 (1988).
17. H. Nakanishi and M. E. Fisher, *Phys. Rev. Lett.* **49**:1565 (1982).
18. S. Dietrich and M. Napiorkowski, *Phys. Rev. A* **43**:1861 (1991).
19. J. S. Rowlinson and B. Widom, *Molecular Theory of Capillarity*, (Clarendon Press, Oxford, 1984), Chap. 3.
20. P.-G. de Gennes, *Rev. Mod. Phys.* **57**:827 (1985).
21. D. E. Sullivan and M. M. Telo da Gama, in *Fluid Interfacial Phenomena*, C. A. Croxton, ed. (Wiley, Chichester, 1986), Chap. 2.

22. To understand how the phase portrait evolves in the limit $A \to -0$, with $B > 0$ fixed, one must take into account that the golf club (Fig. 2) changes to an inverted golf club, for $A \geqslant 0$. However, as long as $A < 0$ (no matter how small) the topology remains as in Fig. 2, but the three branches in the upper right corner converge to a single branch for vanishing A. Thus, for $B \neq 0$ the topology of Fig. 2 makes a jump as a function of A, at $A = 0$.
23. J. O. Indekeu, *Europhys. Lett.* **10**:165 (1989); G. Langie and J. O. Indekeu, *J. Phys. Cond. Matt.* **3**:9797 (1991); W. F. Saam and V. B. Shenoy, *J. Low Temp. Phys.* **101**:225 (1995).
24. M. E. Fisher and A. Jin, *Phys. Rev. B* **44**:1430 (1991); A. Jin and M. E. Fisher, *Phys. Rev. B* **47**:7365 (1993).
25. R. Lipowsky, D. Kroll, and R. K. P. Zia, *Phys. Rev. B* **27**:4499 (1983); E. Brézin, B. I. Halperin, and S. Leibler, *Phys. Rev. Lett.* **50**:1387 (1983).
26. R. Blossey, *Int. J. Mod. Phys.* **9**:3489 (1995); D. Bonn and J. O. Indekeu, *Phys. Rev. Lett.* **74**:3844 (1995).
27. A. O. Parry, *J. Phys. A* **26**:L667 (1993); A. O. Parry and C. J. Boulter, *Mol. Phys.* **87**:501 (1996).
28. C. J. Boulter and J. O. Indekeu, *Phys. Rev. E* **56**:5734 (1997).
29. We comment here on the necessary restriction to $m_1 > -m_0$. There exists a subspace of profiles that cannot be reached, not even with the extension to $l < 0$. It consists of profiles that start at $m_1 < -m_0$ and contain a negative coverage (since the density at the wall is lower than the bulk gas density). The limit of the present construction lies at $l = -\infty$, which corresponds to $m_1 = m_b = -m_0$, and $V(l)$ saturates to the free-energy value associated with that profile. Beyond this limit lies the regime of negative coverage, which plays no significant role in the applications we are interested in.
30. D. W. Jordan and P. Smith, *Nonlinear Ordinary Differential Equations* (Clarendon, Oxford, 1987), Chap. 1.
31. Surface spinodal phenomena are addressed in D. Bonn, H. Kellay and J. Meunier, *Phys. Rev. Lett.* **73**:3560 (1994); for a tutorial see J. O. Indekeu and D. Bonn, *J. Mol. Liq.* **71**:163 (1997).
32. K. Ragil, Ph.D. Thesis, Université Pierre et Marie Curie, Paris VI (1996).
33. The error margin given in ref. 2, 0.03, is the error on the fitted exponent assuming the data points are free of errors. The actual error margin is greater and 0.3 is a reasonable estimate.
34. For a recent detailed study of wetting on curved surfaces, see T. Bieker and S. Dietrich, *Physica A* **252**:85 (1998).